

# Characterization of Zener-Tunneling Drain Leakage Current in High-Dose Halo Implants

Chang-Hoon Choi, Shyh-Horng Yang\*, Gordon Pollack\*, Shashank Ekbote\*, PR Chidambaram\*,  
Scott Johnson\*, Chuck Machala\*, and Robert W. Dutton

Center for Integrated Systems, Stanford University, Stanford, CA 94305, USA

\*Texas Instruments Inc., Dallas, TX 75243, USA

Phone: (650) 723-9484, Fax: (650) 725-7731, E-mail: chchoi@stanford.edu

## Abstract

Degraded junction leakage current in scaled MOSFETs due to enhanced band-to-band tunneling (i.e. local Zener effect) is characterized based on a modified band-to-band tunneling model. To suppress the severe drain leakage current in the presence of high-dose halo implants, the impact of implant conditions on drain leakage current is estimated based on implant induced damage (point defect) profiles.

## 1 Introduction

Gate-induced drain leakage (GIDL) current in MOSFETs is generally ascribed to the band-to-band tunneling between the drain and the body region. As MOSFET scaling continues, gate oxide thickness and doping profiles play a key role in the GIDL current. In particular, as the halo ion-implant is widely used to suppress short channel effects for sub- 100 nm CMOS technology [1], the dopant concentration of the channel region becomes higher than  $1 \times 10^{18} \text{ cm}^{-3}$ , which results in high electric fields ( $> 1 \times 10^6 \text{ V/cm}$ ) between the drain extension and the channel. In the case of such strong electric fields, carrier transitions via the band to band (Zener) and trap-assisted tunneling mechanisms are significant; large drain leakage current by band-to-band tunneling becomes one of the crucial constraints for MOSFET scaling.

## 2 Zener Tunneling Leakage Current

Fig. 1 shows measured drain leakage currents for a 90 nm node NMOS transistor, employing halo implant (boron) with doses of  $4 \times 10^{13}$  and  $6 \times 10^{13} \text{ cm}^{-2}$ . The gate and source are grounded and the measured data is normalized with respect to 1 nA of leakage current. The leakage current rapidly increases with reverse drain bias and the slope is greater for the higher dose ( $6 \times 10^{13} \text{ cm}^{-2}$ ) relative to the lower one ( $4 \times 10^{13} \text{ cm}^{-2}$ ). The increased defect density for the high-dose ion-implantation is a major contributing factor, which can enlarge the local electric field in the reverse bias p-n depletion layer– the so called the local Zener effect [2].

To investigate the origin of the increased leakage currents the Zener probability ( $P$ ) in the presence of local enhancements of the electric field is considered, as given by [2]:

$$P = \frac{qa\eta E}{h} \exp\left(-\frac{\pi^2 a \sqrt{m^*} E_g^2}{h^2 q\eta E}\right) \quad (1)$$

where  $E$  is the local electric field,  $a$  is the lattice constant of Si ( $= 0.543 \text{ nm}$ ),  $h$  is Planck's constant, and  $m^*$  is the electron effective mass ( $= 0.5m_0$ ).  $\eta$  is the field enhancement coefficient with the value between 1 and 3 which depends on precipitate material and other process conditions.

Assuming that  $N(x)$  is the defect (precipitate) density and  $P(x)$  is the local Zener probability at the depth of  $x$ , then the leakage current ( $J$ ) caused by the Zener effects can be estimated as:

$$J \propto qnR^3 \int_0^x N(x)P(x)dx \quad (2)$$

where  $R$  is the radius of the defect and  $n$  is the electron concentration.

This equation implies that the leakage current due to the local Zener effect is a function of the electric field and defect concentration profile, such that the leakage current reaches a peak when defects exist in the region where the electric field is maximized.

To investigate the origin of the large leakage current Zener tunneling probabilities ( $P$ ) for the higher halo dose is 1-order magnitude higher than that for the lower one in Fig. 2, which can be the origin for the large leakage current.

Fig. 3 shows the product of  $N(x)$  and  $P(x)$  and its integrated value along the  $x$  direction to estimate the leakage current ( $J$ ) based on Eq. (2). The defect concentration ( $N(x)$ ) is assumed to be increased from the Si surface in the depth direction. As a result, Fig. 3 (b),(c) show about an order-of-magnitude higher  $N(x)P(x)$  and leakage current for the higher halo dose owing to the higher  $P$ , which is consistent with the experimental data shown in Fig. 1.

## 3 Modeling of Degraded Junction Leakage

To quantify the increased leakage current for high-dose halo implants, device simulation [3] is utilized with a recombination model [4] that includes both trap-assisted tunneling and band-to-band tunneling. In this model the total recombination rate is given by:

$$R = R_{trap} + R_{btt} \quad (3)$$

where  $R_{trap}$  is the recombination rate due to transitions via traps and  $R_{btt}$  is the rate due to the band-to-band tunneling contribution. The  $R_{trap}$  term calculates the excess carrier

concentration due to injected carriers and the tunneling contribution via traps.  $R_{btt}$  originates from Kane's theoretical solution of the Schrödinger equation, given by [4]:

$$R_{btt} = -BE^{2.5}D(E, E_{fn}, E_{fp})exp\left(-\frac{E_0}{E}\right) \quad (4)$$

where  $E$  is the local electric field,  $E_{fn}$  and  $E_{fp}$  are the Fermi levels at the  $n$  and  $p$  sides, and function  $D$  gives the relative positions of the quasi-Fermi levels.  $E_0$  is the characteristic electric field for band-to-band tunneling with a typical value of  $1.9 \times 10^7$  V/cm, which contains the tunneling temperature dependence.

Fig. 4 shows simulated drain leakage currents (lines) compared to measured data (symbols). The solid lines denote the simulated drain leakage currents using the recombination model with typical default parameter values. The dotted lines represent the simulated drain current without the band-to-band tunneling term ( $R_{btt}$ ). However, the conventional  $R_{btt}$  model alone cannot satisfactorily explain the rapid increase in leakage current for high-dose halo implants. To model this phenomenon, the characteristic field in Eq. (4),  $E_0$ , is assumed to be linearly reduced as the body dopant concentration ( $N_A$ ) increases. A modified characteristic field,  $E'_0$ , can be expressed as:

$$E'_0 = E_0 - a(N_A - N_0) \quad (5)$$

where  $a$  is the parameter to determine the characteristic field with respect to body concentration.  $E_0$  is the original characteristic field in Eq. (1) with the value of  $1.9 \times 10^7$  V/cm and  $N_0$  is the reference body dopant concentration for the  $E_0$  value. As a result of using the relationship in Eq. (2), good agreement is achieved as shown in Fig. 5 between the experimental data and the device simulation with the parameters,  $a = 5.5 \times 10^{-12}$  V·cm<sup>2</sup> and  $N_0 = 3 \times 10^{18}$  cm<sup>-3</sup>.

#### 4 Defect Density for Halo Implants

As thermal budgets for modern CMOS technology must be tightly controlled, dopant profiles are mainly dominated by implant damage and interface states. If the amount of primary implant damage is above a critical level, point defects can turn into {311} defects or even into stable dislocation loops, that can cause large leakage current when they are located in a p-n junction under bias conditions [5]. Thus, the defect density profile for a given set of process conditions can provide useful insight concerning leakage current characteristics. Process simulations [?] were performed to observe defect (damage) profiles for different halo implant conditions; the defect-enhanced diffusion model is used to take into account implant damage (point defects) and transient-enhanced diffusion (TED) effects. A Monte-Carlo ion-implant model is employed to consider the atomic structure of the silicon lattice.

Fig. 6(a) shows contours of excess defect density (i.e. interstitial supersaturation ratio) for halo doses of  $4 \times 10^{13}$

cm<sup>-2</sup> and the tilt-angle of 15°, followed by a RTA thermal treatment. The excess defect density ratio is the ratio of the interstitial defect concentration to the equilibrium interstitial concentration ( $C_I/C_I^*$ ). The excess defect density ratio has its minimum near the Si surface since the damaged silicon lattice is restored to the crystalline state, starting from the Si surface over the annealing time. Fig. 6(b) compares simulated defect profiles in the channel direction for different halo conditions. The excess defect density is lower by ~10 % when the halo dose is  $4 \times 10^{13}$  cm<sup>-2</sup>, relative to that of  $6 \times 10^{13}$  cm<sup>-2</sup>; the defect density ratio is reduced by ~15 % when the implant tilt-angle changes from 15 to 45°. This is because high-dose halo implants can result in larger damage to the silicon crystal. In addition, a small implant tilt-angle produces higher dopant concentrations and deeper projected range ( $R_p$ ), compared to large-tilt angle, which leads to damage in the sub-surface junction, farther away from the surface. Since silicon crystal damage by ion-implant adjacent to the silicon surface can be annealed more quickly than the damages in the deeper junction a large implant tilt may produce lower defect densities and lower leakage current. However, to reduce the total off-state leakage current ( $I_{off} = I_{DB} + I_{DS} + I_{DG}$ ), optimization of the halo implant dose and tilt is essential by considering the trade-off between the drain-to-body leakage current ( $I_{DB}$ ) and the drain-to-source (subthreshold) leakage current ( $I_{DS}$ ). For example, too low a dopant concentration in the channel causes severe drain-to-source subthreshold leakage current ( $I_{DS}$ ).

#### 5 Summary

Anomalous large drain leakage current in scaled MOSFETs due to the local Zener effect is characterized using a modified band-to-band tunneling model, in which the characteristic electric field is determined as a function of body concentration. A large tilt halo implant is shown to be more desirable to reduce the implant damage (point defects), since the silicon crystal damage by ion-implant adjacent to the silicon surface can be more easily annealed than in the deeper junction regions during the thermal treatment.

#### Acknowledgment

This project is supported by Texas Instruments Inc., through a customized research under SRC Contract 2001-MJ-966.

#### REFERENCES

- [1] B. Yu and et al., *IEDM Tech. Dig.*, p. 653, 1999.
- [2] K. Ohyu and et al., *IEEE T. ED*, p.1404, Aug. 1995.
- [3] *MEDICI : Two-Dimensional Device Simulation Program*. Synopsys, Inc., 2002.
- [4] G.A.M. Hurkx and et al., *IEEE T. ED*, p.331, Feb. 1992
- [5] J.D. Plummer and et al., *Silicon VLSI Technology: Fundamentals, Practice and Modeling*. Prentice Hall, Inc., 2000.

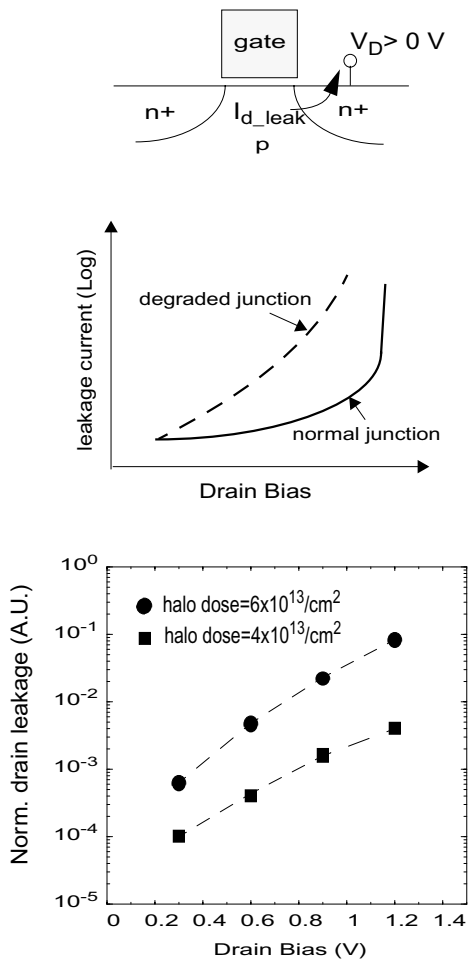


Fig. 1. Measured leakage currents between the drain and the bulk for halo implant (boron) doses of  $4 \times 10^{13}$  and  $6 \times 10^{13}$   $\text{cm}^{-2}$ , implant energy = 10 KeV and tilt-angle = 15. Gate, source and bulk nodes are grounded.

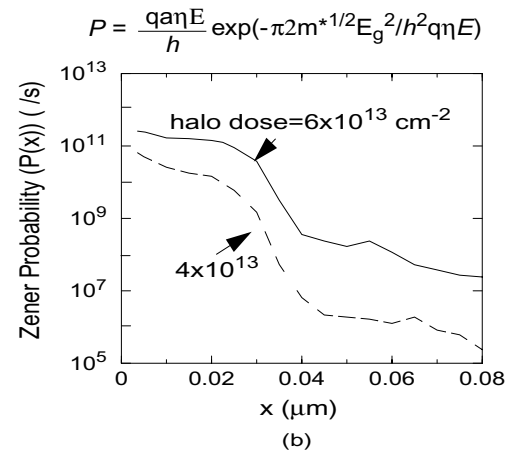
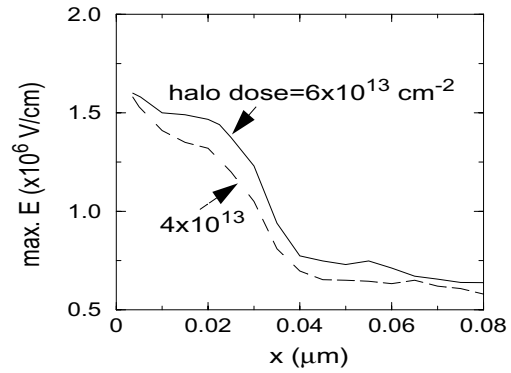
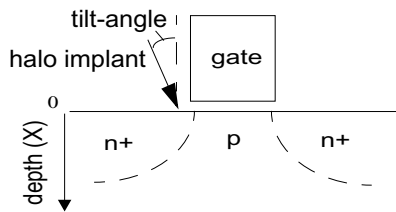
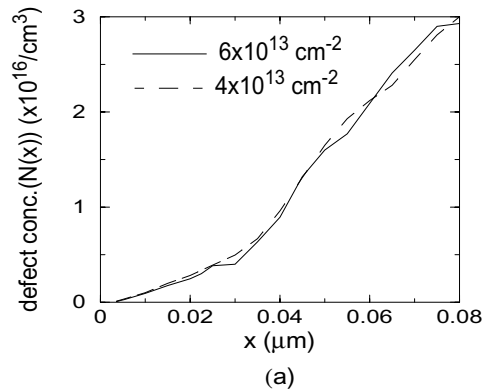
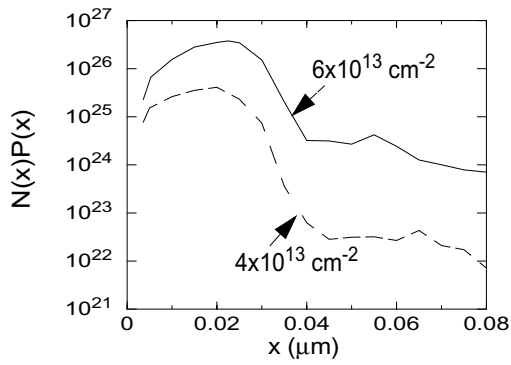


Fig. 2. Zener probabilities along the drain sidewall junction in the depth direction for two halo doses at  $V_{ds}=1.2\text{V}$ ; local electric fields ( $E$ ) to calculate  $P$  are obtained from device simulations. Only  $\sim 10\%$  higher  $E$  causes 1-order magnitude higher  $P$  in  $E$ -field  $> 1 \times 10^6$  V/cm regime, which results in 1-order magnitude higher leakage current in halo dose= $6 \times 10^{13}/\text{cm}^2$ , relative to halo dose= $4 \times 10^{13}/\text{cm}^2$ .





(b)

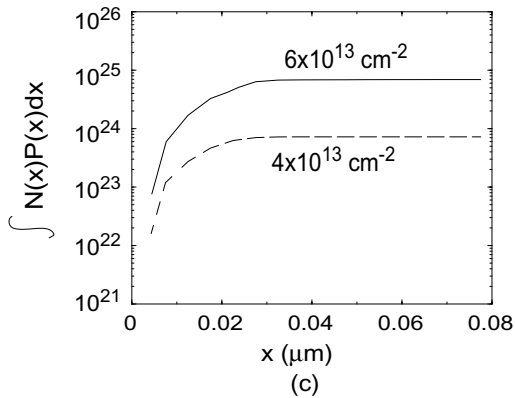


Fig. 3.  $N(x)P(x)$  product and its integration into the  $x$ -direction to estimate the leakage current based on Eq.(2). (a) assumed defect concentration profile ( $N(x)$ ) (b)  $N(x)P(x)$  for different halo doses (c) comparisons of  $N(x)P(x)$  integration.

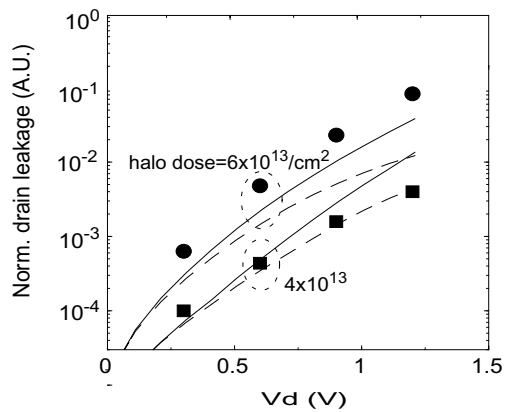


Fig. 4. Simulated drain leakage currents (lines) compared with the experiments (symbols). Solid lines denote simulated leakage currents using the recombination model with the band-to-band tunneling ( $R_{btb}$ ) in Eq. 2, and dotted lines denote simulated leakage current without the band-to-band tunneling term ( $R_{btb}$ ).

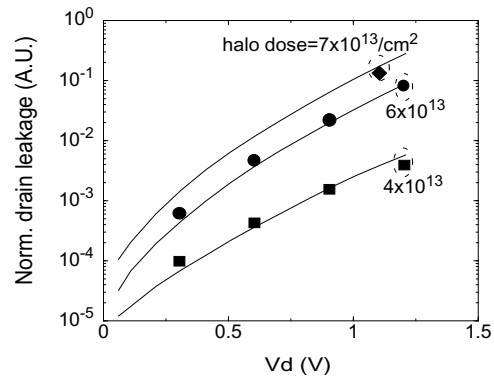
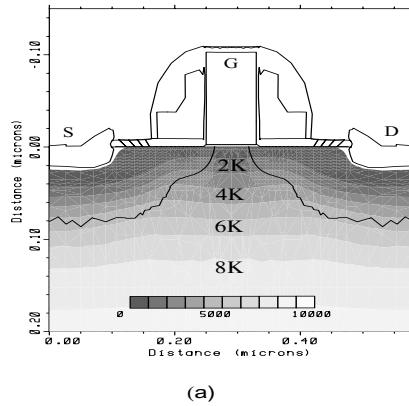
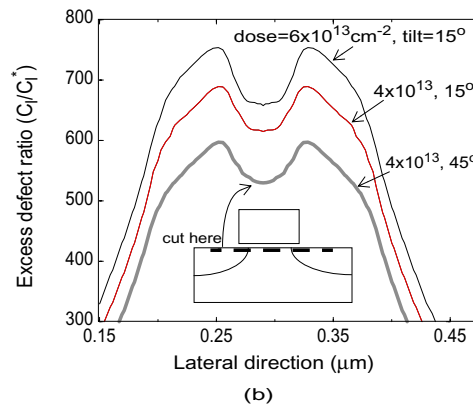


Fig. 5. Comparison between the measured (symbols) and simulated drain leakage currents (lines) based on the modified characteristic field for band-to-band tunneling as a function of the body concentration in Eq. (3).



(a)



(b)

Fig. 6. Simulated point defect profiles of an NMOS by assuming  $L_G = 70$  nm and  $t_{ox} = 1.5$  nm, (a) contours of excess defect density ratio (interstitial supersaturation ratio,  $C_i/C_i^*$ ) for halo dose =  $4 \times 10^{13}$   $\text{cm}^{-2}$  and tilt-angle =  $15^\circ$ . (b) distribution of excess defect density ratio between the source/drain extension and the channel region for different halo doses and tilt angles.